INTERNATIONAL JOURNAL FOR NUMERICAL METHODS IN FLUIDS, VOL. 12, 287–296 (1991)

SHORT COMMUNICATION

NUMERICAL PREDICTION OF TURBULENT FLOW OVER A TWO-DIMENSIONAL RIDGE

F. N. MOUZAKIS AND G. C. BERGELES

Laboratory of Aerodynamics, National Technical University of Athens, 42 Patission Str., 10682 Athens, Greece

SUMMARY

Predictions are presented of the two-dimensional turbulent flow over a triangular ridge. The time-averaged Reynolds equations are written in an orthogonal curvilinear co-ordinate system and transformed to finite difference form after discretization in physical space. Turbulence is simulated by the two-equation κ–ε model of turbulence. In the first part of the paper the basics of the numerical method are presented and in the second part comparisons are made between predictions and available laboratory data. Therefore the validity and reliability of the method as well as its flexibility in treating complex recirculating flows are assessed. Results of engineering significance are presented of the effect of the ridge slope on the length of the recirculation region and on the overspeed factor on top of the ridge.

KEY WORDS Finite difference method Turbulent recirculating flow Curvilinear orthogonal co-ordinate system Hybrid upwind differencing scheme Turbulence model

INTRODUCTION

Knowledge of the turbulent flow around surface obstacles is of significant importance in various branches of engineering since such flows are common in both natural and technological environments. Analytical methods which have been reported, such as the analytical perturbation theory of Jackson and Hunt[1] and the Sykes method[2] based on the matched asymptotic expansion theory, are applicable only in non-recirculating flows around gently sloping hills. Finite difference methods for the solution of the Navier–Stokes equations expressed in Cartesian co-ordinates offer an attractive alternative to previous methods; however, these methods suffer from numerical diffusion errors owing to the misalignement of the local velocity vector with respect to the co-ordinate line.

Recent developments in the field of finite differencing, such as the skew upwind differencing scheme of Raithby *et al.*[3] and the quadratic upstream interpolation scheme of Leschziner,[4] proved to be successful in reducing numerical diffusion errors, although some non-physical oscillations and numerical instabilities have been noticed as a result of the negative coefficients that appear in the finite difference equations. Also, developments in turbulence modelling , such as the Reynolds stress model, led to better predictions of the velocity profile, but this was not reflected in any improvement in predicting the reattachment length.[5]

This paper addresses the technological problem of turbulent flow around a ridge. The problems of the application of the boundary conditions, which are encountered if a Cartesian co-ordinate

0271–2091/91/030287–10$05.00

Received April 1988
Revised February 1990

system is used, are avoided by using a boundary-fitted orthogonal curvilinear co-ordinate system. The use of such a grid also minimizes errors due to numerical diffusion. The method employed has already been tested for the cases of gently sloping hills and escarpments by Bergeles;[6] however, in the hills examined the recirculating region was rather limited and it is further extended here in flows with large recirculating area.

MATHEMATICAL FOUNDATION AND NUMERICAL SOLUTION

Equations and boundary conditions

The time-averaged Reynolds equations, which express the steady state incompressible turbulent flow in a two-dimensional flow field, can be written in an orthogonal curvilinear co-ordinate system (ξ, η) as follows:

continuity equation

$$\frac{1}{h_\xi h_\eta}\frac{\partial}{\partial \xi}(\rho u h_\eta) + \frac{1}{h_\xi h_\eta}\frac{\partial}{\partial \eta}(\rho v h_\xi) = 0, \tag{1}$$

momentum and energy conservation equation

$$\frac{1}{h_\xi h_\eta}\frac{\partial}{\partial \xi}(\rho u \phi h_\eta) - \frac{1}{h_\xi h_\eta}\frac{\partial}{\partial \xi}\left(\mu_\phi \frac{h_\eta}{h_\xi}\frac{\partial \phi}{\partial \xi}\right) + \frac{1}{h_\xi h_\eta}\frac{\partial}{\partial \eta}(\rho v \phi h_\xi) - \frac{1}{h_\xi h_\eta}\frac{\partial}{\partial \eta}\left(\mu_\phi \frac{h_\xi}{h_\eta}\frac{\partial \phi}{\partial \eta}\right) - S_\phi = 0, \tag{2}$$

where ϕ stands for the time-mean values of the contravariant velocity components u, v, the turbulent kinetic energy κ and the turbulence dissipation rate ε, S_ϕ is the source term whose analytical expressions are shown in Table I, and h_ξ, h_η are the spatially varying metric coefficients of the curvilinear co-ordinate system. The orthogonal co-ordinate system fitted to the shape of the ridge is shown in Figure 1.

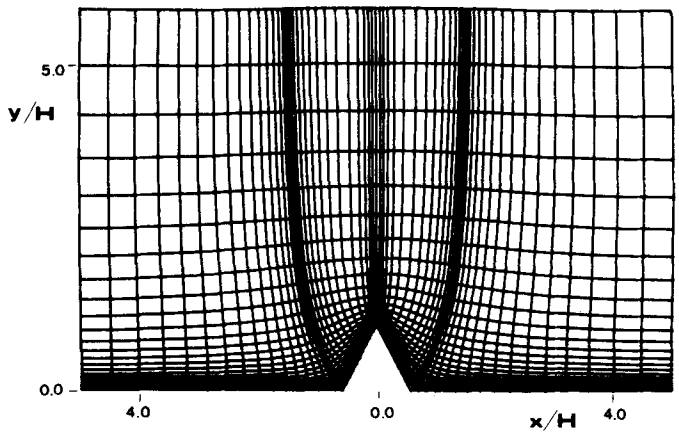

Figure 1. Orthogonal curvilinear co-ordinate system around a ridge with a side slope of 2 (enlarged part close to the ridge crest)

Table I. Analytical expressions for the source terms of the governing equations

ϕ	S_ϕ	μ_ϕ
u	$-\frac{1}{h_\xi}\frac{\partial p}{\partial \xi}-\frac{\rho uv}{h_\xi h_\eta}\frac{\partial h_\xi}{\partial \eta}+\frac{\rho v^2}{h_\xi h_\eta}\frac{\partial h_\eta}{\partial \xi}+\frac{1}{h_\xi h_\eta}\frac{\partial}{\partial \xi}\left[\mu_\phi \frac{h_\eta}{h_\xi}\left(\frac{\partial u}{\partial \xi}+\frac{2v}{h_\eta}\frac{\partial h_\xi}{\partial \eta}\right)\right]$ $+\frac{1}{h_\xi h_\eta}\frac{\partial}{\partial \eta}\left[\mu_\phi h_\xi\left(\frac{1}{h_\xi}\frac{\partial v}{\partial \xi}-\frac{v}{h_\xi h_\eta}\frac{\partial h_\eta}{\partial \xi}-\frac{u}{h_\xi h_\eta}\frac{\partial h_\xi}{\partial \eta}\right)\right]$ $+\frac{\mu_\phi}{h_\xi h_\eta}\left(\frac{1}{h_\xi}\frac{\partial v}{\partial \xi}+\frac{1}{h_\eta}\frac{\partial u}{\partial \eta}-\frac{v}{h_\xi h_\eta}\frac{\partial h_\eta}{\partial \xi}-\frac{u}{h_\xi h_\eta}\frac{\partial h_\xi}{\partial \eta}\right)\frac{\partial h_\xi}{\partial \eta}-\frac{2\mu_\phi}{h_\xi h_\eta}\left(\frac{1}{h_\eta}\frac{\partial v}{\partial \eta}+\frac{u}{h_\xi h_\eta}\frac{\partial h_\eta}{\partial \xi}\right)\frac{\partial h_\eta}{\partial \xi}$	$\mu+\mu_t$
v	$-\frac{1}{h_\eta}\frac{\partial p}{\partial \eta}-\frac{\rho uv}{h_\xi h_\eta}\frac{\partial h_\eta}{\partial \xi}+\frac{\rho u^2}{h_\xi h_\eta}\frac{\partial h_\xi}{\partial \eta}+\frac{1}{h_\xi h_\eta}\frac{\partial}{\partial \eta}\left[\mu_\phi \frac{h_\xi}{h_\eta}\left(\frac{\partial v}{\partial \eta}+\frac{2u}{h_\xi}\frac{\partial h_\eta}{\partial \xi}\right)\right]$ $+\frac{1}{h_\xi h_\eta}\frac{\partial}{\partial \xi}\left[\mu_\phi h_\eta\left(\frac{1}{h_\eta}\frac{\partial u}{\partial \eta}-\frac{u}{h_\xi h_\eta}\frac{\partial h_\xi}{\partial \eta}-\frac{v}{h_\xi h_\eta}\frac{\partial h_\eta}{\partial \xi}\right)\right]$ $+\frac{\mu_\phi}{h_\xi h_\eta}\left(\frac{1}{h_\eta}\frac{\partial u}{\partial \eta}+\frac{1}{h_\xi}\frac{\partial v}{\partial \xi}-\frac{u}{h_\xi h_\eta}\frac{\partial h_\xi}{\partial \eta}-\frac{v}{h_\xi h_\eta}\frac{\partial h_\eta}{\partial \xi}\right)\frac{\partial h_\eta}{\partial \xi}-\frac{2\mu_\phi}{h_\xi h_\eta}\left(\frac{1}{h_\xi}\frac{\partial u}{\partial \xi}+\frac{v}{h_\xi h_\eta}\frac{\partial h_\xi}{\partial \eta}\right)\frac{\partial h_\xi}{\partial \eta}$	$\mu+\mu_t$
κ	$\mu_\phi\left[2\left(\frac{1}{h_\xi}\frac{\partial u}{\partial \xi}+\frac{v}{h_\xi h_\eta}\frac{\partial h_\xi}{\partial \eta}\right)^2+2\left(\frac{1}{h_\eta}\frac{\partial v}{\partial \eta}+\frac{u}{h_\xi h_\eta}\frac{\partial h_\eta}{\partial \xi}\right)^2\right.$ $\left.+\left(\frac{1}{h_\xi}\frac{\partial v}{\partial \xi}+\frac{1}{h_\eta}\frac{\partial u}{\partial \eta}-\frac{v}{h_\xi h_\eta}\frac{\partial h_\eta}{\partial \xi}-\frac{u}{h_\xi h_\eta}\frac{\partial h_\xi}{\partial \eta}\right)^2\right]-\rho\varepsilon \quad (=G-\rho\varepsilon)$	$\frac{\mu+\mu_t}{\sigma_\kappa}$
ε	$C_1 G\frac{\varepsilon}{\kappa}-C_2\frac{\varepsilon^2}{\kappa}\rho$	$\frac{\mu+\mu_t}{\sigma_\varepsilon}$

Turbulence closure

The two-equation turbulence model of Jones and Launder[7] for the turbulent kinetic energy κ and its rate of dissipation ε is employed. Particular attention is given to the region near the wall; the need for a fine numerical grid is avoided in this region by use of the wall function treatment. The wall functions represent the physical fluid properties in a Couette flow.[8] In such a flow, in the near-wall region, when the wall pressure gradient is taken into account, the following equations are derived:

$$p_+ y_+ = \frac{y}{\tau_w}p', \qquad \tau = \tau_+ \tau_w = 1 + p_+ y_+, \qquad \kappa = \frac{\tau}{\rho c_\mu^{0\cdot 5}},$$

where $p' = \mathrm{d}p/\mathrm{d}x$ is the pressure gradient and κ is the turbulent kinetic energy. From the above equations we obtain the following expression for the non-dimensional parameter y_+:

$$y_+ = \frac{\rho y}{\mu}\sqrt{\left(\kappa c_\mu^{0\cdot 5} - \frac{yp'}{\rho}\right)},$$

which is incorporated into the normally used wall function expression.[8]

Another modification introduced into the turbulence model is an expression for the κ–ε turbulence model parameter c_μ (normally taken as constant with a value of 0·09). Such an expression is suggested by Rodi,[9] who, correlating experimental data, proposed a function $c_\mu = f(P/\varepsilon)$, where P and ε are the production and dissipation of turbulence kinetic energy respectively. Although the above function was suggested for improving the reliability of the κ–ε model in predicting weak shear flows, it also improved the results in the present application where the flow is strongly perturbed.

The numerical grid

For the numerical solution of the governing partial differential equations (1) and (2), an orthogonal curvilinear co-ordinate system fitted to the whole integration domain is needed. Such a co-ordinate system is obtained, following the method of Theodoropoulos *et al.*,[10] by solving the following set of Laplace equations using a finite differencing scheme:

$$\frac{\partial}{\partial\xi}\left(h\frac{\partial x}{\partial\xi}\right)+\frac{\partial}{\partial\eta}\left(\frac{1}{h}\frac{\partial x}{\partial\eta}\right)=0, \qquad \frac{\partial}{\partial\xi}\left(h\frac{\partial y}{\partial\xi}\right)+\frac{\partial}{\partial\eta}\left(\frac{1}{h}\frac{\partial y}{\partial\eta}\right)=0, \tag{3}$$

where h is the scale factor ratio (i.e. $h = h_\eta/h_\xi$) which is given by

$$h(\xi,\eta)=\sqrt{\left(\frac{(\partial x/\partial\eta)^2+(\partial y/\partial\eta)^2}{(\partial x/\partial\xi)^2+(\partial y/\partial\xi)^2}\right.}. \tag{4}$$

Numerical solution of the equations

All the governing equations can be cast into the general form of equation (2) for different values of the source term S_ϕ and the coefficient μ_ϕ as shown in Table I. By integration according to the SIMPLE method,[11] the transport equation is transformed into the finite difference form

$$(A_P^\phi - SP_P^\phi)\phi_P = A_E^\phi\phi_E + A_W^\phi\phi_W + A_N^\phi\phi_N + A_S^\phi\phi_S + SU_P^\phi, \tag{5}$$

where

$$A_P^\phi = A_E^\phi + A_W^\phi + A_N^\phi + A_S^\phi.$$

This method has been extensively used by various workers in a variety of applications.[6,11–13]

The grid-independent results which are presented have been obtained with a numerical grid of 97×35 points. The calculations have been performed on a CDC Cyber 171-8 mainframe computer, where the code required 9000 CPU seconds execution time and 410 000 B loader field length.

PRESENTATION AND DISCUSSION OF RESULTS

Detailed measurements of the flow field around a triangular ridge have been reported by Arya and Shipman.[14] The experiments were conducted in a wind-tunnel and the mean velocity and turbulence measurements were made with hot wire anemometers in conjunction with boundary-layer-type crossed hot film probes.

The orthogonal curvilinear co-ordinate system that covers the whole integration domain and fits to the shape of the ridge is shown in Figure 1. The slope of the ridge side is 2:1 and its height is equal to one-tenth of the boundary layer thickness of the undisturbed approaching flow. For the complete simulation of the experiments the velocity profile at the inflow boundary was selected to

be the same as that measured by Arya and Shipman[14] at the same location upstream of the ridge.

When examining cases where the flow field boundaries retain continuity of the second spatial derivative and a decent numerical grid is used, the assumption that the grid lines are straight between two adjacent grid nodes is a reasonable one and in accordance with the discretization process of equation (2).

However, in cases where the boundary slopes do not retain continuity, such as on the top of the ridge, the above assumption leads immediately to a considerable underestimation of the curvature of the grid lines, particularly for the computational cells near the ridge peak.

The curvatures of the grid lines, i.e. $(1/\Delta x_i)(\partial x_i/\partial x_j)$, are usually estimated by the simple formula $\Delta(\Delta x_i)/\Delta s$, where Δx_i is the distance between two adjacent grid points along the i-direction and Δs is area of the cell around the point where the curvature is being calculated. The magnitudes of Δx_i, however, are accurately estimated when the constant-η lines over the ridge peak are approximated by a cubic spline (which passes through the computed grid points). This procedure, in conjunction with the use of a fine mesh around the sharp ridge peak, improved the accuracy of the results compared to experiment.

The predictions, by examination of the pressure coefficient (C_p) contour diagram in Figure 2, show that the presence of the ridge has an effect on the flow that starts at least 8 ridge heights upstream (location of the 10% contour) and causes the approaching flow to respond to an adverse pressure gradient. Also seen are the strong streamwise pressure gradient on top of and immediately after the ridge and the flow recovery to the ambient pressure downstream of the ridge. A parabolic type of flow can only been seen after 14 ridge heights past the ridge, where the pressure across the flow is small and constant (location of 5% contour value).

From the streamline plots in Figure 3, the cavity region that starts from the ridge top has a length of $10H$ whereas its maximum height is approximately $1{\cdot}5H$, where H is the ridge height. Beyond the cavity a new wall shear layer starts developing whose thickness increases with distance downstream of the ridge.

In the experiment of Arya and Shipman[14] the cavity region, which was established by smoke visualization, was found to extend $13H$ in the longitudinal direction with a maximum height of $2{\cdot}5H$. From their velocity measurements, however, it seems that the length of the recirculation region cannot be larger than $8H$, since already at this location a positive velocity is measured. In the measurements reported by Bergeles and Athanassiadis,[15] where the recirculating bubble

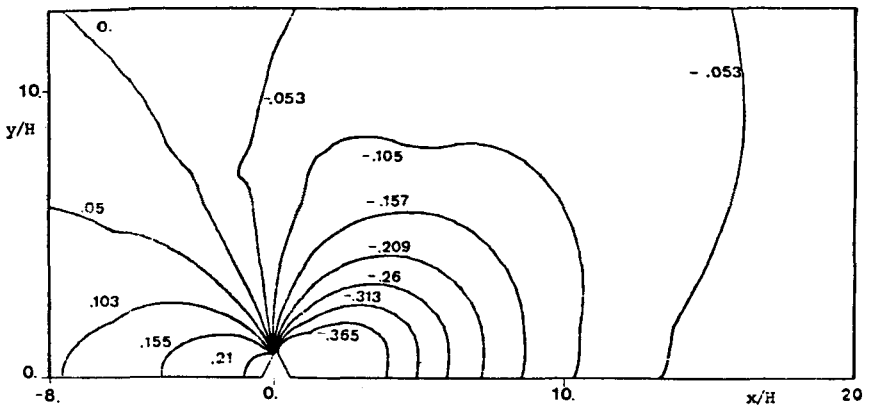

Figure 2. Pressure coefficient contour diagram: $C_p = (p - p_\infty)/\frac{1}{2}\rho U_\infty^2$

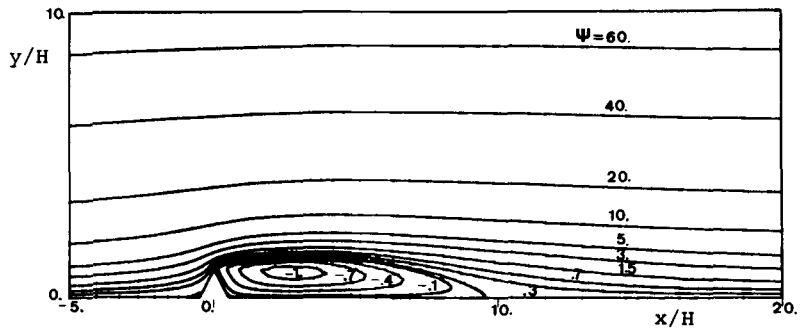

Figure 3. Streamlines of the flow over the ridge (ambient velocity 8 m s^{-1})

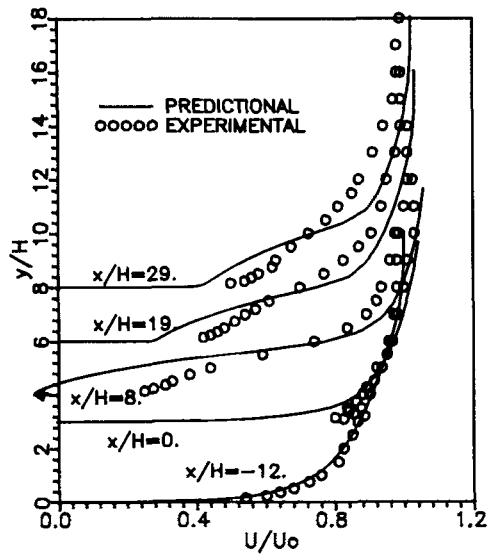

Figure 4. Velocity profiles at various locations relative to the ridge

around a surface-mounted square obstacle was established in a similar way (smoke and tufts), the recirculating bubble had a height of 2·2H and extended 11H downstream. Thus the differences in the cavity dimensions that appear between the predictions and the measurements are primarily due to the uncertainty of the measuring method, whose accuracy according to Arya and Shipman[14] is anything within 15%. Furthermore, from the numerical point of view, the inevitable non-orthogonality that appears at the top of the ridge, and consequently affects the arithmetic solution, as well as the turbulence model utilized, which is known to have the tendency to underpredict the length of the recirculating regions in flows where steep velocity gradients appear,[5] are possible sources of error.

In Figure 4 comparisons are made between the predicted (also in Figure 6) and measured velocity profiles at various locations. At $x/H = -12$ the experimental data were used as a boundary condition for the numerical solution and consequently they coincide. Around the top of

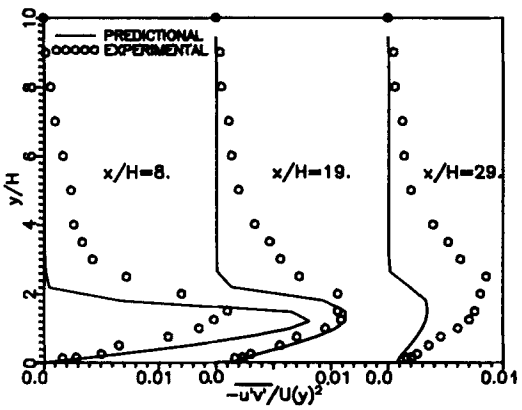

Figure 5. Reynolds stress profiles at various distances relative to the ridge

the ridge ($x/H = 0$) there is agreement between predicted and measured profiles, except just over the top of the ridge where the velocity is slightly underpredicted.

At $x/H = 8$ the predicted flow is characterized by a negative mean velocity in the wall region, since this position is within the predicted cavity region. The reverse flow is predicted to have a height of $0{\cdot}5H$ at this location. However, the measuring method with hot wire anemometers is incapable of detecting reverse flow and consequently in that region the experimental procedure fails to give the correct flow direction; thus the result conflicts with the fact that the flow visualization technique gave a cavity length of $13H$. Outside the bubble region ($y/H > 1{\cdot}4$) the velocity field is in agreement with the measurements.

In Figure 5 the predicted and measured Reynolds stress profiles are compared. The comparison indicates reasonable universality of the κ–ε model for the near-wall flow but severe underprediction of the stresses in wake-type flows. This reinforces the previous argument as regards the rate of velocity recovery in the wake region.

Results for a constant c_μ-value (0·09) have also been obtained. The major effect of the use of a function for estimating c_μ instead of using a constant value is assessed by inspection of Figure 6, which presents the velocity profile results for the case where c_μ is constant. The cavity bubble length is found to be shorter, approximately $9H$, while the rate of velocity recovery is further underpredicted.

Another point that proved to be essential in this study was the modifications utilized for the correct estimation of the curvature of the grid lines near the peak of the ridge. The results obtained without the above modification (c_μ was constant also) are also presented in Figure 6 in the form of velocity profiles. The cavity bubble length is further decreased (almost $8H$) while the predicted velocities differ considerably from the experimental data.

Further application of the method for flows over triangular ridges with side slopes ranging between 1 and 0·125 shows that the slope of the side wall of the ridges is a basic parameter for many flow characteristics, such as the velocity overspeed, the dimensions of the recirculating bubble and the extent of upstream pressure effects.

In Figure 7 the mean velocity profiles for four different ridges with varying side slope and for two locations relative to the ridge are shown. The decrease of the velocity deficit with smaller slope is obvious. As shown in Figure 8, with the decrease of side slope the length of the recirculation zone is drastically decreased; however, as the side slope increases beyond a value of 2 the length of the cavity is becoming independent of the side slope. In the same figure the

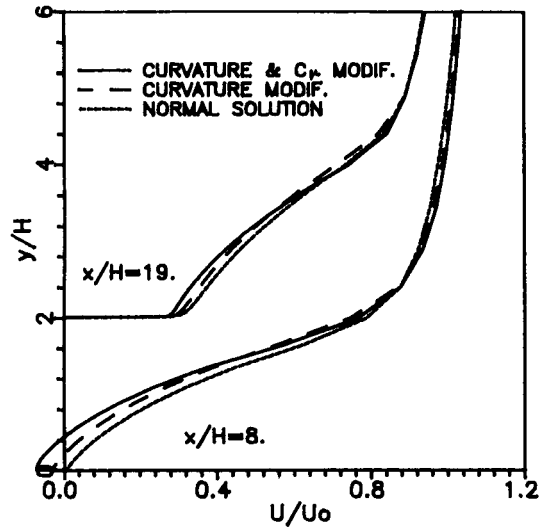

Figure 6. Comparison of velocity profiles at various locations relative to the ridge between different numerical solutions

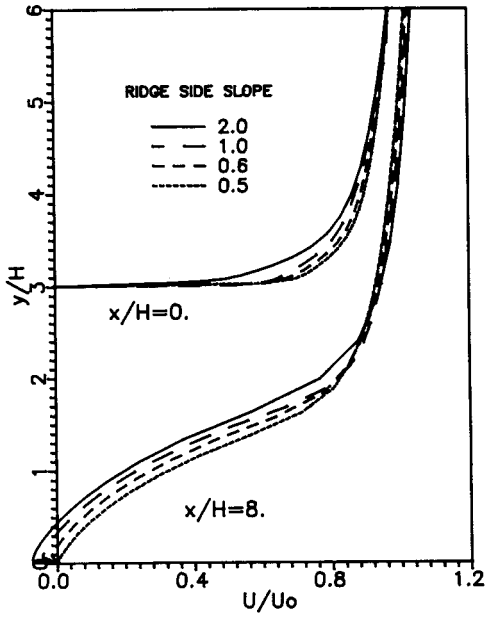

Figure 7. Velocity profiles at various locations relative to the ridge for ridges with different side slope

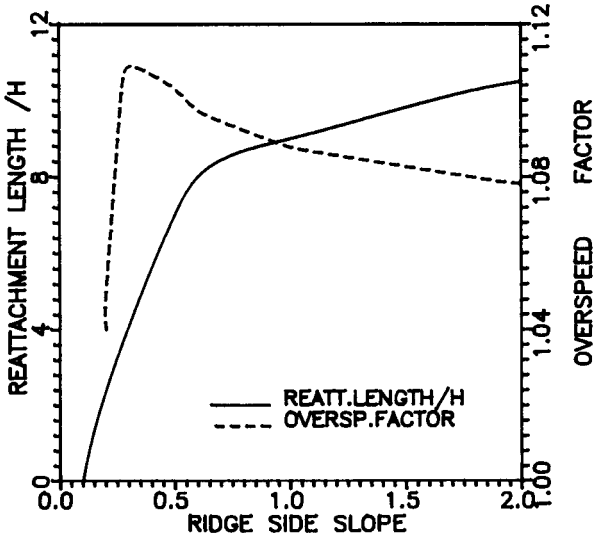

Figure 8. Reattachment length and overspeed factor (at $x/H = 0$ and $y/H = 1{\cdot}5$ relative to the ridge) versus ridge side slope

overspeed factor, namely the ratio of the velocity $0{\cdot}5H$ above the ridge top to the velocity at the same elevation in the undisturbed boundary layer, is also presented. The results confirm that gently sloping hills produce a higher overspeeding factor on top and that there must be a maximum value of velocity overspeed at slopes around 0·4.

CONCLUSIONS

This paper has presented results of a numerical study in solving the two-dimensional time-averaged Reynolds equations for incompressible steady state flows over a ridge. The equations are written in an orthogonal curvilinear co-ordinate system and are solved by use of a finite differencing scheme. The set of governing equations is closed with the addition of the two-equation κ–ε turbulence model. The method uses orthogonal curvilinear co-ordinate systems, which guarantees simplicity in the application of the boundary conditions, accurate representation of the shape of the boundary geometry and reduction of the numerical diffusion. Also, the introduction of accurate estimation of the curvature of the grid lines near the points of the second spatial derivative discontinuity on the boundaries turned out to be of major importance, since it had a direct effect on the dimension of the recirculating region. The use of a variable turbulent parameter c_μ according to the formula prescribed by Rodi[9] also improved the reliability of the results.

The validity of the method has been assessed by comparing the predictions with measurements for the flow over a ridge. The method predicts the measurements reasonably accurately. The differences that have been found are attributed to the inevitable non-orthogonality which appears at the integration cell just over the ridge top and to the turbulence model deficiency in regions of steep velocity gradients and strongly curved streamlines. However, differences between predictions and measurements may also be attributed to high experimental uncertainties associated with the measuring technique in flows of high levels of turbulence.

APPENDIX: NOMENCLATURE

A_i^ϕ	coefficient in finite difference equations linking the central node P with the adjacent node i (= E, S, N, W) for the dependent variable ϕ.
S_ϕ	source term for the dependent variable ϕ
x, y	Cartesian co-ordinates
ξ, η	co-ordinate distances in the curvilinear system
h_ξ, h_η	metric coefficients for the directions ξ and η respectively of the co-ordinate system
h	ratio of metric coefficients of the curvilinear co-ordinate system, h_η/h_ξ
u, v	velocity components along the directions ξ and η respectively of the co-ordinate system
p	pressure
ρ	density of the fluid
μ	dynamic viscosity of the fluid
κ, ε	turbulent kinetic energy and its rate of dissipation respectively
τ	shear stress in boundary layer
$-\rho\overline{u'v'}$	Reynolds shear stress
μ_t	turbulent viscosity of the fluid
p_+	dimensionless pressure gradient parameter[8]
y_+	dimensionless normal distance co-ordinate[8]

σ_κ, σ_ε	diffusion constants of κ and ε respectively
τ_+	ratio of local to wall values of shear stress
C_μ, C_1, C_2	constants of the κ–ε turbulence model
H	height of the ridge

Subscripts

P, N, S, E, W	central and neighbouring nodes of the grid
ϕ	dependent variable (i.e. u, v, κ, ε)
t	turbulent flow
w	wall conditions
∞	free stream conditions

REFERENCES

1. P. Jackson and J. Hunt, 'Turbulent wind flow over a low hill', *Q. J. R. Meteorol. Soc.*, **101**, 929–955 (1975).
2. R. Sykes, 'An asymptotic theory of incompressible turbulent boundary layer flow over a small hump', *J. Fluid Mech.*, **101**, 647–670 (1980).
3. R. Raithby, C. Hackman and A. Strong, 'Numerical predictions of flows over backward facing steps', *Int. j. numer. methods fluids*, **4**, 711–724 (1984).
4. M. Leschziner, 'Practical evaluation of three finite difference schemes for the computation of steady-state recirculating flows', *Comput. Methods Appl. Mech. Eng.*, **23**, 293–312 (1980).
5. J. McGuirk, C. Papadimitriou and A. Taylor, 'Reynolds stress model calculations of two-dimensional plane and axisymmetric recirculating flows', *Proc. Fifth Symp. on Turbulence, Cornell University, Ithaca*, Cornell University, Ithaca, NY, 1985, p. 20.12a.
6. G. Bergeles, 'Numerical calculation of turbulent flow around two-dimensional hills', *J. Wind Eng. Ind. Aerodyn.*, **21**, 307–321 (1985).
7. W. Jones and B. Launder, 'The prediction of laminarization with a two-equation model of turbulence', *Int. J. Heat Mass Transfer*, **15**, 301 (1972).
8. B. Launder and D. Spalding, *Mathematical Models of Turbulence*, Pergamon, Oxford, 1972.
9. W. Rodi, 'Turbulence models and their application in hydraulics. A state of the art review', International Association of Hydraulic Research, The Netherlands, June 1980.
10. T. Theodoropoulos, G. Bergeles and N. Athanasiadis, 'Orthogonal grid generation in two dimensional space', *Proc. Fourth Int. Conf. on Numerical Methods in Laminar and Turbulent Flow*, Pineridge Press, Swansea, July 1985, pp. 1747–1758.
    Fourth Int. Conf. on Numerical Methods in Laminar and Turbulent Flow, Swansea. July 1985.
11. S. Patankar and D. Spalding, 'A calculation procedure for heat, mass and momentum transfer in three-dimensional parabolic flows', *Int. J. Heat Mass Transfer*, **15**, 1787 (1972).
12. G. Bergeles, A. Gosman and B. Launder, 'Double row discrete hole cooling: an experimental and numerical study', *J. Eng. Power*, **102**, 498–503 (1980).
13. S. Patankar, D. Basu and S. Alpay, 'Prediction of the three-dimensional velocity field of a turbulent deflected jet', *J. Fluids Eng.*, **99**, 758 (1977).
14. S. Arya and M. Shipman, 'An experimental investigation of flow and diffusion in the disturbed boundary layer over a ridge. I. Mean flow and turbulence structure', *Atmos. Environ.*, **15**, 1173–1184 (1981).
15. G. Bergeles and N. Athanassiadis, 'The flow past a surface mounted obstacle', *ASME J. Fluids Eng.*, **105**, 461–463 (1983).